

Supernovae and their host galaxies – II. The relative frequencies of supernovae types in spirals

A. A. Hakobyan,^{1*} T. A. Nazaryan,¹ V. Zh. Adibekyan,² A. R. Petrosian,¹
L. S. Aramyan,¹ D. Kunth,³ G. A. Mamon,³ V. de Lapparent,³ E. Bertin,³
J. M. Gomes² and M. Turatto⁴

¹Byurakan Astrophysical Observatory, 0213 Byurakan, Aragatsotn province, Armenia

²Centro de Astrofísica da Universidade do Porto, Rua das Estrelas, 4150-762 Porto, Portugal

³Institut d'Astrophysique de Paris (UMR 7095: CNRS & UPMC), 98bis Bd Arago, 75014 Paris, France

⁴INAF – Osservatorio Astronomico di Padova, Vicolo dell'Osservatorio 5, 35122 Padova, Italy

Accepted 2014 August 5. Received 2014 August 2; in original form 2014 May 27

ABSTRACT

We present an analysis of the relative frequencies of different supernova (SN) types in spirals with various morphologies and in barred or unbarred galaxies. We use a well-defined and homogeneous sample of spiral host galaxies of 692 SNe from the Sloan Digital Sky Survey in different stages of galaxy–galaxy interaction and activity classes of nucleus. We propose that the underlying mechanisms shaping the number ratios of SNe types can be interpreted within the framework of interaction-induced star formation, in addition to the known relations between morphologies and stellar populations. We find a strong trend in behaviour of the $N_{\text{Ia}}/N_{\text{CC}}$ ratio depending on host morphology, such that early spirals include more Type Ia SNe. The $N_{\text{Ibc}}/N_{\text{II}}$ ratio is higher in a broad bin of early-type hosts. The $N_{\text{Ia}}/N_{\text{CC}}$ ratio is nearly constant when changing from normal, perturbed to interacting galaxies, then declines in merging galaxies, whereas it jumps to the highest value in post-merging/remnant galaxies. In contrast, the $N_{\text{Ibc}}/N_{\text{II}}$ ratio jumps to the highest value in merging galaxies and slightly declines in post-merging/remnant subsample. The interpretation is that the star formation rates and morphologies of galaxies, which are strongly affected in the final stages of interaction, have an impact on the number ratios of SNe types. The $N_{\text{Ia}}/N_{\text{CC}}$ ($N_{\text{Ibc}}/N_{\text{II}}$) ratio increases (decreases) from star-forming to active galactic nuclei (AGN) classes of galaxies. These variations are consistent with the scenario of an interaction-triggered starburst evolving into AGN during the later stages of interaction, accompanied with the change of star formation and transformation of the galaxy morphology into an earlier type.

Key words: supernovae: general – galaxies: spiral – galaxies: interactions – galaxies: stellar content – galaxies: active.

1 INTRODUCTION

There is a widespread consensus that different kinds of observables of galaxies are related directly to the different stellar populations and to star formation. These observables range from the overall morphology, disturbance due to interaction, presence of bar, activity classes of nucleus and occurrence of supernovae (SNe) of various types.

Different levels of activity in the central region of galaxies can be powered by either accretion on to a supermassive black hole (SMBH; e.g. Hopkins & Quataert 2010), or combination of SMBH induced activity with a burst of circumnuclear massive star formation (e.g. Muñoz Marín et al. 2007), or mostly massive star

formation alone (e.g. Das et al. 2012). Association of active galactic nuclei (AGN) with circumnuclear star formation is common in many bright Seyfert (Sy) galaxies (e.g. Knapen 2005; Popović et al. 2009) and is supported by modelling of AGN-triggered star formation (e.g. Silk & Norman 2009), and/or the onset of star formation with subsequently fuelled AGN (e.g. Davies et al. 2007; Hopkins 2012). The star formation in AGN host galaxies is not concentrated primarily in the nuclear regions, but is distributed over scales of at least several kiloparsecs (e.g. Kauffmann et al. 2003, 2007).

A possible mechanism to explain the co-evolution of an AGN and its host galaxy is that both nuclear and extended activity are triggered by interacting/merging of galaxies (e.g. Storchi-Bergmann et al. 2001; Kuo et al. 2008; Sabater, Best & Argudo-Fernández 2013). The produced gas inflow not only forms massive stars in the central region,

* E-mail: hakobyan@bao.sci.am

but also fuels the SMBH in the centre of galaxies (e.g. Di Matteo, Springel & Hernquist 2005). There also exists the possibility, depending on accretion rate, that enhanced star formation in discs does not correlate with the nuclear activity but with interaction (e.g. Jarrett et al. 2006; Das et al. 2012). An additional possibility is that gravitational instabilities in the disc of barred galaxies can cause gas transfer to the central regions of galaxies (e.g. Wyse 2004). In this respect, the presence of bars can play an important role in the star formation of galaxies (e.g. Ellison et al. 2011).

The triggered bursts of star formation strongly affect the observed numbers of SNe (e.g. Bressan, Della Valle & Marziani 2002; Petrosian et al. 2005; Habergham, James & Anderson 2012; Kangas et al. 2013) in addition to the known relations between the rate of various SN types and the stellar content of galaxies with different morphologies (e.g. Cappellaro, Evans & Turatto 1999; Mannucci et al. 2005; Li et al. 2011). Core-Collapse (CC) SNe, whose progenitors are thought to be young massive stars (e.g. Turatto 2003; Smartt 2009; Anderson et al. 2012), are observationally classified in three major classes, according to the strength of lines in optical spectra (e.g. Filippenko 1997): Type II SNe show hydrogen lines in their spectra, while Types Ib and Ic do not, with Type Ib SNe showing helium and Type Ic SNe showing neither hydrogen nor helium. There are two proposed channels for stripping the hydrogen and helium envelopes: (1) massive Wolf-Rayet stars with large ($M \geq 30 M_{\odot}$) main-sequence masses that experience strong mass-loss (e.g. Heger et al. 2003); (2) lower mass binaries stripped through interaction by a close companion (e.g. Podsiadlowski, Joss & Hsu 1992). Therefore, the progenitors of SN Ibc¹ may be more massive than those of normal SN II (8 – 16 M_{\odot} ; Smartt 2009) or explode in regions of higher metallicity (e.g. Heger et al. 2003). Due to short-lived massive progenitors (< 0.1 Gyr; Schaller et al. 1992), CC SNe are considered as good tracers of recent star formation in galaxies (e.g. Petrosian & Turatto 1990, 1995; Cappellaro et al. 1999; Petrosian et al. 2005; Anderson & James 2009; Hakobyan et al. 2009; Anderson et al. 2012; Crowther 2013; Kangas et al. 2013; Shao et al. 2014). Thermonuclear SNe, alias Type Ia SNe, result from stars of different ages (> 0.5 Gyr), with even the shortest lifetime progenitors having much longer lifetime than the progenitors of CC SNe (e.g. Maoz & Mannucci 2012). Their rates are described as a sum of two terms, one depending on the current star formation rate (SFR) and another on the total stellar mass (e.g. Mannucci et al. 2005; Scannapieco & Bildsten 2005; Hakobyan et al. 2011; Li et al. 2011). Type Ia SNe are associated less tightly to star formation in spirals and irregulars (e.g. James & Anderson 2006).

Several authors have studied the number ratios (e.g. Prantzos & Boissier 2003; Boissier & Prantzos 2009) and spatial distributions (e.g. Bartunov, Makarova & Tsvetkov 1992; van den Bergh 1997; Förster & Schawinski 2008; Anderson & James 2009; Hakobyan et al. 2009) of different SN types in large numbers of galaxies. None of these studies have attempted to categorize the hosts according to their activity classes of nucleus and interaction. Nevertheless, other authors have shown that the number ratios (e.g. Bressan et al. 2002; Petrosian et al. 2005; Shao et al. 2014) and distributions of SNe (e.g. Petrosian & Turatto 1990; Petrosian et al. 2005; Hakobyan

2008; Wang, Deng & Wei 2010; Kangas et al. 2013) might be different in galaxies with varying activity classes. For example, Bressan et al. (2002) showed that the ratio $N_{\text{Ibc}}/N_{\text{II}}$ between the total numbers of SNe Ibc and SNe II reflects metallicity, age, fraction of binary systems, and initial mass function (IMF) shape, which might be quite different in galaxies with various activity classes of nuclei. They also found that the ratio $N_{\text{Ibc}}/N_{\text{II}}$ measured in Sy galaxies exceeds that in normal host galaxies by a factor of 4. Studying a sample of CC SNe in galaxies hosting AGN, Petrosian et al. (2005) and Hakobyan (2008) found that the SNe in active/star-forming (SF) galaxies are more centrally concentrated than those in normal galaxies. Herrero-Illana, Pérez-Torres & Alberdi (2012) modelled the radial distribution of SNe in the nuclear starbursts of M 82, Arp 220, and Arp 299A galaxies, and interpreted the results as evidence of galaxy-galaxy interactions that are expected to trigger massive star formation down to the central kiloparsec region of galaxies. In addition, Habergham et al. (2012) presented the results of a re-analysis of Habergham, Anderson & James (2010) with increased statistics and found a remarkable excess of CC SNe within the central regions of disturbed galaxies, i.e., in galaxies showing signs of merger-triggered starbursts in the nuclei.

The locations of SNe in multiple systems of galaxies have also been studied (e.g. Petrosian & Turatto 1995; Navasardyan et al. 2001; Nazaryan et al. 2013). There is an indication that the SN rate is higher in galaxy pairs compared with that in groups (Navasardyan et al. 2001). In addition, SNe Ibc are located in pairs interacting more strongly than pairs containing SNe Ia and II (Nazaryan et al. 2013). These results are considered to be related to the higher SFR in strongly interacting systems.

However, the aforementioned studies suffer from poor statistics, as well as strong biases in the SNe and their host galaxies samples. In our first paper of this series (Hakobyan et al. 2012, hereafter Paper I), we have created a large and well-defined data base that combines extensive new measurements and a literature search of 3876 SNe and their 3679 host galaxies located in the sky area covered by the Sloan Digital Sky Survey (SDSS) Data Release 8 (DR8). This data base is much larger than previous ones, and is expected to provide a homogeneous set of global parameters of SN hosts, including morphological classifications and measures of activity classes of nuclei. In addition, we have analysed and discussed many selection effects and biases, which usually affect the studies of SNe. For more details, the reader is referred to Paper I.

In this paper, we investigate the correlations between SNe number ratios ($N_{\text{Ia}}/N_{\text{CC}}$, $N_{\text{Ibc}}/N_{\text{II}}$, and $N_{\text{Ic}}/N_{\text{Ib}}$) and other observable parameters of host galaxies. We present an analysis of the SNe number ratios in spiral galaxies with different morphologies and with or without bars. In addition, we use a well-defined and homogeneous sample of host galaxies with various levels of interaction to explore the numbers of SNe resulting from star formation in their host galaxies as a function of morphological disturbances. Furthermore, we perform a statistical study of SNe discovered in galaxies with different activity classes of nuclei [e.g. SF, composite (C), low-ionization nuclear emission-line region (LINER), or Sy] using relative frequencies of the various SN types. We reveal and discuss the underlying mechanisms shaping the number ratios of SNe types within the framework of interaction-induced star formation, in addition to the well-known relations between morphologies and stellar populations.

This is the second paper of a series and the outline is as follows. Section 2 introduces sample selection. In Section 3, we give the results and discuss all the statistical relations. Our conclusions

¹ By SN Ibc, we denote stripped-envelope SNe of Type Ib, Ic, and mixed Ib/c whose specific subclassification is uncertain.

Table 1. Types of 14 SNe unclassified in Paper I.

SN name	Type ^a	Ref.
1988E	II pec :	Murdin & Green (1988)
1988ab	Ia :	Richmond et al. (1998)
1988ac	Ib/c ?	Richmond et al. (1998)
1992bf	Ia pec :	Conley et al. (2008)
1992bu	Ib/c ?	Anderson et al. (2011)
1993R	Ia pec :	Filippenko & Matheson (1993)
1999gs	Ia :	Foley & Mandel (2013)
2000ft	II	Alberdi et al. (2006)
2002bp	Ia pec :	Silverman et al. (2012)
2004cs	Ia pec :	Foley et al. (2013)
2005co	Ia	Blanc et al. (2005)
2008hl	Ib/c ?	Foley & Mandel (2013)
2009az	IIP	Kankare (2013)
2010cr	Ia :	Milne et al. (2013)

^aSNe 1988ac and 2008hl are classified as CC SNe in Richmond et al. (1998) and Foley & Mandel (2013), respectively. However, taking into account the local environments (see Crowther 2013, and references therein) of this SNe, we list them as probable Type Ib/c.

are summarized in Section 4. Throughout this paper, we adopt a cosmological model with $\Omega_m = 0.27$, $\Omega_\Lambda = 0.73$, and a Hubble constant is taken as $H_0 = 73 \text{ km s}^{-1} \text{ Mpc}^{-1}$ (Spergel et al. 2007), both to conform to the values used in our data base.

2 SAMPLE SELECTION

The current investigation is based upon the total sample of SNe and their host galaxies presented in Paper I². This data base contains spectroscopic classes, accurate coordinates, and offsets from galaxy nucleus of 3876 SNe (72 SNe I, 1990 SNe Ia, 234 SNe Ibc, 870 SNe II³, and 710 unclassified SNe)⁴ from the coverage of SDSS DR8. The last SN included in the total sample of Paper I is SN 2011bl (Nayak et al. 2011), discovered on 2011 April 5. Using the SDSS multiband images, photometric, and spectral data, Paper I also provides accurate coordinates, heliocentric redshifts, morphological types, activity classes of nuclei, apparent g -band magnitudes, major axes (D_{25}), axial ratios (b/a), and position angles of the SNe host galaxies. In addition, it is noted whether a host has a bar, a disturbed disc, or is part of an interacting or merging system.

In Paper I, we have shown that the total sample of SNe is largely incomplete beyond $100 \pm 3 \text{ Mpc}$: the distributions of SNe of Types Ibc and II are similar and display a sharp decline beyond this value (see fig. 14 in Paper I). Type Ia SNe, because of their comparatively high luminosity and the presence of dedicated surveys, are discovered at much greater distances than CC SNe. Thus, to avoid biasing the current sample against or in favour of one of the SN types, we truncate the sample to distances $\leq 97 \text{ Mpc}$.

² The parameters of several SNe and their host galaxies were revised in Aramyan et al. (2013).

³ Note that in SN II, we include Types IIP, IIL, I Ib, and IIn.

⁴ All the uncertain (‘?’ or ‘?’) and peculiar (‘pec’) classifications are flagged in table 7 of Paper I. Types I, Ia, and II include also a few SNe classified from the light curve only.

Table 2. New morphological types of 20 host galaxies, which were not attributed precise Hubble subclasses in Paper I, but were simply labelled as ‘S’.

Galaxy ^a	Morph. ^b	Bar
J001911.00+150622.7	Sm ?	B
J005740.42+434732.0	Sc :	B
J021030.84+022005.7	Sb :	
J030211.42–010959.3	Sm ?	
J030258.52–144904.4	Sm ?	
J043400.04–083445.0	Sbc :	
J073656.63+351431.9	Sc	
J074726.42+265532.5	Sm ?	
J083824.00+254516.3	Sbc :	
J094315.30+361707.1	Sdm :	
J095100.34+200420.4	Sdm :	
J105846.90+592912.5	Sb ?	
J112830.77+583342.9	Sc ?	
J112833.38+583346.4	Sc ?	
J115913.13–013616.0	Sm :	
J145407.71+423253.1	Sm :	
J221930.27+292316.9	Sc :	
J231925.09+055421.6	Sb :	
J235125.02+200641.9	Sbc :	B
PGC 71868 ^c	Sb :	

^aHost galaxy SDSS designation.

^bSymbol ‘:’ indicates that the classification is doubtful and ‘?’ indicates that the classification is highly uncertain.

^cAn alternative name is mentioned since there is no photometric object in the SDSS at the position of the galaxy.

An additional restriction to SNe discoveries is needed, because Type Ibc SNe were labelled as ‘I pec’ types during observations before 1986. Therefore, we also limit the sample to SNe discovered since 1986. It is important to take into account the fact that SNe Ia explode in all morphological types of galaxies, while CC SNe explode mostly in spiral and irregular hosts (e.g. van den Bergh, Li & Filippenko 2005; Hakobyan et al. 2008, 2012). Therefore, to exclude SNe type biasing due to host-galaxy morphology, we further restrict the sample to SNe detected in spiral galaxies (including S0/a types). Note that irregular hosts are not selected, because they show neither prominent nuclei nor clear discs, on which we focus in this article.

After these restrictions, we look through the current literature for available information on the spectroscopic types of the 31 unclassified SNe of Paper I. Table 1 presents the collected types for 14 SNe with the respective references. In addition, Leaman et al. (2011) have reported that there was no SN at the position of SN 2003dl. Therefore, we remove SN 2003dl from our analysis. The remaining 16 SNe without spectroscopic classification (1989ac, 1991bk, 1997bm, 1998cf, 1998cp, 2004ad, 2005cd, 2006A, 2007cd, 2007gq, 2007kc, 2008iv, 2009gt, 2010dh, 2010ha, and 2010lo) are also removed from the sample.

After these operations, we are left with a sample of 692 SNe within 608 host galaxies. In addition, we morphologically classify 20 host galaxies of 27 SNe, which were without precise Hubble subclasses (labelled as ‘S’) in Paper I. The results are presented in Table 2. Table 3 displays the distribution of all SNe types among the various considered spiral types for their host galaxy. In Table 4, we

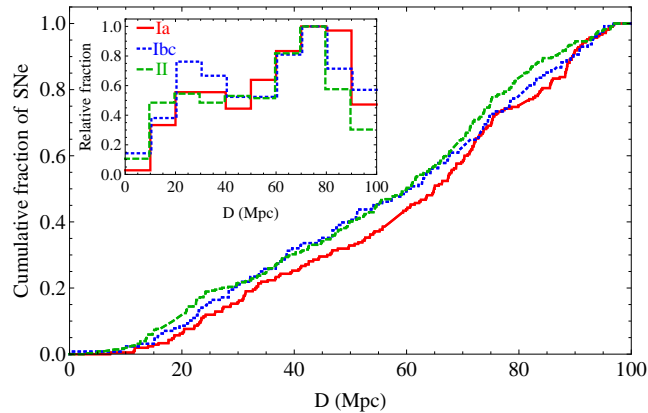


Figure 1. Cumulative and relative (inset) fractions of 692 SNe (Ia – red solid, Ib/c – blue dotted, and II – green dashed) in S0/a – Sm galaxies as a function of distance, discovered in the time interval between 1986 January and 2011 April.

Table 3. Numbers of SNe discovered since 1986, and with a distance ≤ 97 Mpc, according to morphological type of host galaxies (S0/a – Sm). Among all the SNe types, there are 40 uncertain (‘?’ or ‘?’) and 49 peculiar (‘pec’) classifications.

	S0/a	Sa	Sab	Sb	Sbc	Sc	Scd	Sd	Sdm	Sm	All
Ia	27	14	20	33	40	46	13	13	3	1	210
Ib	0	0	1	5	6	14	4	0	2	0	32
Ib/c	1	3	1	3	6	9	1	2	1	1	28
Ic	0	1	1	9	22	17	6	8	1	3	68
II	2	7	7	41	75	125	35	32	18	12	354
All	30	25	30	91	149	211	59	55	25	17	692

also present the distribution of SNe in barred or unbarred galaxies, for each spiral type.

Fig. 1 shows the cumulative and relative fractions of the 692 SNe with Types Ia, Ib/c, and II as a function of distance. We underline that SNe classified as Ib/c are included in the computation of $N_{\text{Ib/c}}$, but are omitted when computing N_{Ib} and N_{Ic} ; and SNe classified as IIb and IIc are included in the computation of N_{II} . The Kolmogorov–Smirnov (KS) goodness-of-fit test shows that the distributions in Fig. 1 are not significantly different from each other ($P_{\text{KS}}^{\text{Ia,Ib/c}} = 0.35$, $P_{\text{KS}}^{\text{Ia,II}} = 0.14$, $P_{\text{KS}}^{\text{Ia,CC}} = 0.20$, $P_{\text{KS}}^{\text{Ib/c,II}} = 0.88$, and $P_{\text{KS}}^{\text{Ib,Ic}} = 0.63$) and could thus be drawn from the same parent distribution of distances. Therefore, our samples of SNe and their host galaxies should not be strongly affected by any of the redshift-dependent bias discussed in Paper I.

We additionally define for all 608 host galaxies their level of morphological disturbance with the possible presence of signs of interactions and mergers. We do this by visual inspection of the combined SDSS g -, r -, and i -band images of the hosts, and comparison with the colour images of the simulations of equal-mass gas-rich disc mergers in Lotz et al. (2008). The comparison with the simulations is done in order to identify the stages of interaction for all the host galaxies. We define four categories of SN host disturbances: normal (hosts without any visible disturbance in their morphological structure), perturbed (hosts with visible morphological disturbance, but without long tidal arms, bridges, or destruction of spiral patterns), interacting (hosts with obvious signs

Table 4. Numbers of SNe in barred and unbarred galaxies among the various morphological types.

	S0/a	Sa	Sab	Sb	Sbc	Sc	Scd	Sd	Sdm	Sm	All
Unbarred	21	19	21	59	104	173	48	15	11	11	482
Barred	9	6	9	32	45	38	11	40	14	6	210
All	30	25	30	91	149	211	59	55	25	17	692

of galaxy–galaxy interaction), merging (hosts with evidence of an ongoing merging process; see e.g. Lambas et al. 2012), and post-merging/remnant (single galaxies that exhibit signs of a past interaction, with a strong or already relaxed disturbance, see e.g. Ellison et al. 2013 and Lotz et al. 2008, respectively). Fig. 2 shows images of typical examples of SNe host galaxies with different levels of disturbances⁵.

The visual inspection of the combined SDSS g -, r -, and i -band images is performed by one of the co-authors (TAN) only, in order to insure a uniform classification. To test this classification, a subset of 100 host galaxies is randomly selected from the classified sample, and re-classified by another co-author (AAH). By comparing both classifications for the 100 galaxy subset, we measure a difference of disturbance class by one unit in only 5 per cent of the galaxies, suggesting that there are no major systematic biases in the full classification. Table 5 shows the distribution of SNe in the 608 host galaxies of different morphological types among the different disturbance classes.

In addition, using the standard diagnostic diagram (Baldwin, Phillips & Terlevich 1981, hereafter BPT) presented in Paper I, we were able to determine different activity classes of nuclei of SNe host galaxies. Inspecting the SDSS DR10 (Ahn et al. 2014), we find additional spectra of 12 host galaxies from the Baryon Oscillation Spectroscopic Survey. Using the method described in Paper I, we also classify 11 of them (see Table 6). In the BPT diagram, the hosts with SDSS nuclear spectra include 46 narrow-line AGN (10 Sy and 36 LINER), 143 SF, and 43 C galaxies with 268 SNe in total. The spectra of 31 galaxies with 31 SNe did not meet the criteria on signal-to-noise ratio of the BPT diagnostic (see Paper I) and thus were not analysed. In total, the activity classes of nuclei of 345 galaxies with 393 SNe were not determined due to absence or poor quality (nine spectra have bad flux calibration or bad redshift determination) of their SDSS spectra. Table 7 displays the distribution of SNe in hosts with different activity classes of nuclei among the various morphological types.

3 RESULTS AND DISCUSSION

In this section, we examine the $N_{\text{Ia}}/N_{\text{CC}}$, $N_{\text{Ib/c}}/N_{\text{II}}$, and $N_{\text{Ic}}/N_{\text{Ib}}$ ratios of the different types of SNe as a function of the host galaxy properties (morphology, presence of bar, disturbance, and activity class of nucleus). In the second column of Table 8, we show the calculated number ratios of SN types for all hosts of types S0/a–Sm. The errors of number ratios are calculated using the approach of Cameron (2011).

The relative frequencies of SNe types presented in the second

⁵ The full table of disturbance levels for 608 individual hosts is only available online.

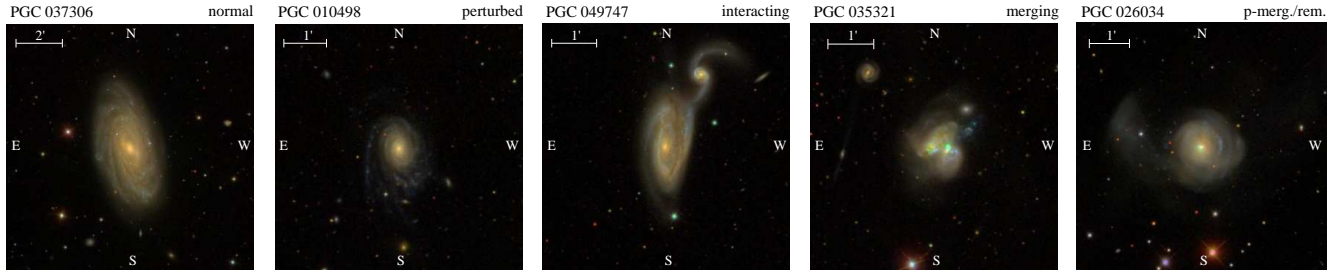


Figure 2. SDSS images representing examples of different levels of disturbances of SNe host galaxies. The Principal Galaxy Catalogue (PGC) objects’ identifiers and levels of disturbances are listed at the top. In all images, north is up and east to the left.

Table 5. Numbers of SNe in galaxies with different disturbance levels among the different morphological types.

	S0/a	Sa	Sab	Sb	Sbc	Sc	Scd	Sd	Sdm	Sm	All
Normal	22	13	18	63	104	151	35	39	15	10	470
Perturbed	0	5	4	20	33	41	20	15	9	2	149
Interacting	3	1	6	3	9	7	3	1	1	4	38
Merging	0	0	0	2	2	12	1	0	0	0	17
p-merg./rem.	5	6	2	3	1	0	0	0	0	1	18
All	30	25	30	91	149	211	59	55	25	17	692

Table 6. New activity classes of nuclei for 11 host galaxies which were listed without classification in Paper I.

Galaxy ^a	BPT
J075126.19+140113.6	LINER
J075923.61+162516.7	SF
J094041.64+115318.1	C
J095619.16+164952.2	SF
J100157.94+554047.8	LINER
J103710.21+123909.2	SF
J110312.95+110436.3	SF
J120236.52+410315.0	SF
J134913.75+351526.2	C
J150821.40+215245.3	SF
J155452.10+210700.0	SF

^aHost galaxy SDSS designation.

column of Table 8 are consistent with previously published values. The ratio of Type Ia to CC SNe in our sample is $0.44^{+0.04}_{-0.03}$, which is close to 0.40 ± 0.04 in Boissier & Prantzos (2009) and 0.40 ± 0.08 obtained from the local SNe sample of Smartt et al. (2009). The $N_{\text{Ibc}}/N_{\text{II}}$ ratio in our study is $0.36^{+0.04}_{-0.03}$, which is similar to 0.31 ± 0.04 in Boissier & Prantzos (2009), 0.33 ± 0.05 in Hakobyan (2008), ~ 0.33 in Hamuy (2003), 0.42 ± 0.09 in Smartt et al. (2009), ~ 0.35 in Smith et al. (2011), and also is similar to those obtained from ratios of CC SN rates in spiral galaxies (e.g. Mannucci et al. 2005; Hakobyan et al. 2011; Li et al. 2011). Finally, our result for $N_{\text{Ic}}/N_{\text{Ib}}$ ratio is $2.12^{+0.48}_{-0.42}$, consistent within larger error bars with 1.53 ± 0.35 in Boissier & Prantzos (2009), 2.0 ± 0.8 in Smartt et al. (2009), and ~ 2.1 in Smith et al. (2011).

Table 7. Numbers of SNe in galaxies with different activity classes of nuclei among the various morphological types. The activity classes are available for only 232 hosts among the sample of 608 host galaxies.

	S0/a	Sa	Sab	Sb	Sbc	Sc	Scd	Sd	Sdm	Sm	All
SF	3	3	4	12	27	42	26	28	11	5	161
C	1	2	2	9	9	27	6	0	1	0	57
Sy	2	0	0	3	3	2	0	0	0	0	10
LINER	3	2	3	10	12	10	0	0	0	0	40
All	9	7	9	34	51	81	32	28	12	5	268

Table 8. The number ratios of SN types ($N_{\text{Ia}}/N_{\text{CC}}$, $N_{\text{Ibc}}/N_{\text{II}}$, and $N_{\text{Ic}}/N_{\text{Ib}}$) in all spiral galaxies and in two morphological subsamples, and the significance value P_{B} of the difference between the ratios in the two subsamples. The total number of SNe is 692 in 608 host galaxies.

	All	S0/a–Sbc	Sc–Sm	P_{B}
$N_{\text{Ia}}/N_{\text{CC}}$	$0.44^{+0.04}_{-0.03}$	$0.70^{+0.08}_{-0.07}$	$0.26^{+0.04}_{-0.03}$	3×10^{-9}
$N_{\text{Ibc}}/N_{\text{II}}$	$0.36^{+0.04}_{-0.03}$	$0.45^{+0.08}_{-0.06}$	$0.31^{+0.05}_{-0.04}$	0.05
$N_{\text{Ic}}/N_{\text{Ib}}$	$2.12^{+0.48}_{-0.42}$	$2.75^{+0.98}_{-0.82}$	$1.75^{+0.53}_{-0.44}$	0.22

3.1 Dependence of relative frequencies of SNe types on host morphology

In Table 9, we present the distribution of number ratios of SN types according to the morphological classification of the host galaxies. Here, we do not calculate the $N_{\text{Ic}}/N_{\text{Ib}}$ ratio due to insufficient number of Ib and Ic SNe in each morphological bin (see also Table 3). The values of $N_{\text{Ia}}/N_{\text{CC}}$ and $N_{\text{Ibc}}/N_{\text{II}}$ as a function of morphological type are shown in Fig. 3.

As can be seen from the left-hand panel of Fig. 3, there is a strong trend in the behaviour of $N_{\text{Ia}}/N_{\text{CC}}$ depending on host-galaxy morphological types, such that early-type spirals include proportionally more Type Ia SNe. As shown in Table 8, the difference between the number ratios of $N_{\text{Ia}}/N_{\text{CC}}$ in two broad morphology bins, i.e., early-type (S0/a–Sbc) and late-type (Sc–Sm) spirals, is statistically significant. The significance value P_{B} is calculated using Barnard’s exact test⁶, which compares the pairs of numbers rather than the number ratios. A similar behaviour of the relative frequencies of SNe types was found by Boissier & Prantzos

⁶ Barnard’s test (Barnard 1945) is a non-parametric test for 2×2 contingency tables, often considered more powerful than Fisher’s exact test.

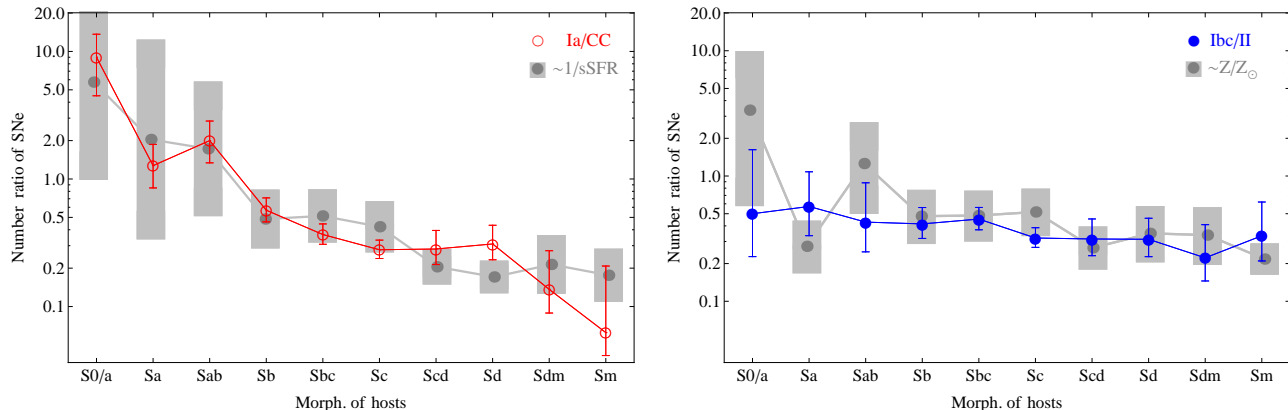


Figure 3. Relative frequency of SNe types as a function of host-galaxy morphology. The number ratio of Type Ia to CC SNe is presented with red open circles (left-hand panel), while the ratio of Types Ibc to II SNe is presented with blue filled circles (right-hand panel). The mean values of $1/s\text{SFR}$ (left-hand panel) and Z/Z_{\odot} (right-hand panel) of host galaxies are presented with dark grey circles. The light grey vertical bars reflect errors of the mean values. These distributions are shifted (not scaled) towards the vertical axis to visually fit the $N_{\text{Ia}}/N_{\text{CC}}$ and $N_{\text{Ibc}}/N_{\text{II}}$ distributions, respectively.

Table 9. The number ratios of SN types ($N_{\text{Ia}}/N_{\text{CC}}$ and $N_{\text{Ibc}}/N_{\text{II}}$) according to morphological classification of host galaxies. The total number of SNe is 692 in 608 host galaxies.

	S0/a	Sa	Sab	Sb	Sbc	Sc	Scd	Sd	Sdm	Sm
$N_{\text{Ia}}/N_{\text{CC}}$	$9.00^{+4.64}_{-4.51}$	$1.27^{+0.59}_{-0.42}$	$2.00^{+0.85}_{-0.66}$	$0.57^{+0.14}_{-0.11}$	$0.37^{+0.08}_{-0.06}$	$0.28^{+0.05}_{-0.04}$	$0.28^{+0.11}_{-0.07}$	$0.31^{+0.12}_{-0.08}$	$0.14^{+0.14}_{-0.05}$	$0.06^{+0.15}_{-0.02}$
$N_{\text{Ibc}}/N_{\text{II}}$	$0.50^{+1.12}_{-0.27}$	$0.57^{+0.51}_{-0.24}$	$0.43^{+0.45}_{-0.18}$	$0.41^{+0.15}_{-0.10}$	$0.45^{+0.11}_{-0.08}$	$0.32^{+0.07}_{-0.05}$	$0.31^{+0.14}_{-0.08}$	$0.31^{+0.15}_{-0.09}$	$0.22^{+0.19}_{-0.08}$	$0.33^{+0.29}_{-0.12}$

(2009), who considered luminosity instead of morphological type. These authors found that brighter galaxies host proportionally more Ia SNe than CC SNe. Their sample consists of 582 SNe in galaxies with $V_{\text{hel}} < 5000 \text{ km s}^{-1}$ ($\lesssim 70 \text{ Mpc}$) and morphological types corresponding to spirals (S0 to Sd) and irregulars (Irr).

Scannapieco & Bildsten (2005) specified that in spiral galaxies, N_{Ia} is a linear combination of the SFR and the total stellar mass (M_*). In addition, it is well known that N_{CC} is proportional to the SFR (e.g. Mannucci et al. 2005). Thus, $N_{\text{Ia}}/N_{\text{CC}}$ is expected to depend linearly on M_*/SFR . To qualitatively demonstrate the relation between the $N_{\text{Ia}}/N_{\text{CC}}$ ratio and the specific SFR ($s\text{SFR} \equiv \text{SFR}/M_*$) of host galaxies, we also display in the left-hand panel of Fig. 3 the distribution of $1/s\text{SFR}$ as a function of morphology, as dark grey circles. These values are calculated as the mean over morphological types. The $s\text{SFR}^7$ values are extracted for the host galaxies of 253 SNe with available spectra in the SDSS DR10. The light grey vertical bars in the left-hand panel of Fig. 3 are the errors of the mean values of $1/s\text{SFR}$ for each bin. The whole distribution is shifted (not scaled) towards the vertical axis to visually match the $N_{\text{Ia}}/N_{\text{CC}}$ distribution. As for $N_{\text{Ia}}/N_{\text{CC}}$, there is a strong trend in the distribution of $1/s\text{SFR}$, such that the $s\text{SFR}$ of host galaxies systematically increases from early- (high-mass or high-luminosity) to late-type (low-mass or low-luminosity) spirals. Here, we share the view with Boissier & Prantzos (2009) that massive (early-type) spirals have, on average, lower $s\text{SFR}$ because of

their smaller gas fractions (e.g. Boissier et al. 2001). In this picture, the behaviour of $N_{\text{Ia}}/N_{\text{CC}}$ versus morphology is a simple reflection of the behaviour of $1/s\text{SFR}$ versus morphological type of galaxies.

The right-hand panel of Fig. 3 presents the distribution of the relative frequency of Types Ibc to II SNe versus host’s morphology. The distribution is nearly flat and shows no apparent dependence on the morphological types. In linear units, the $N_{\text{Ibc}}/N_{\text{II}}$ ratio is slightly decreasing when host morphology becomes of later type. Therefore, when we divide the host sample into two broad morphology bins, the difference between the number ratios in these bins becomes significant (see Table 8). The trend is similar for $N_{\text{Ic}}/N_{\text{Ib}}$, such that early-type spirals include proportionally more Type Ic than Type Ib SNe. But the difference in the relative frequencies of these SNe types is not significant (see Table 8) probably due to the small number statistics in the Types Ib and Ic SNe. Thus, in comparison with the $N_{\text{Ia}}/N_{\text{CC}}$ ratio, the $N_{\text{Ibc}}/N_{\text{II}}$ ratio shows weaker variation with morphology of the hosts.

In general, the $N_{\text{Ibc}}/N_{\text{II}}$ ratio depends on metallicity, age, the fraction of binary systems etc. (e.g. Bressan et al. 2002; Eldridge, Izzard & Tout 2008; Eldridge, Langer & Tout 2011; Smith et al. 2011). To qualitatively examine the relationship between this ratio and metallicity, we use the extracted global galaxy metallicities⁸ available for only 196 CC SNe hosts from the SDSS DR10. In the right-hand panel of Fig. 3, the mean values of global metallicity and their uncertainties are represented by dark grey circles and light grey vertical bars, respectively. Again, the

⁷ The SDSS best-fitting $s\text{SFR}$ values were estimated on extinction-corrected $ugriz$ model magnitudes scaled to the i -band c -model magnitude, using the publicly available Flexible Stellar Population Synthesis code (FSPS; Conroy, Gunn & White 2009).

⁸ The method of best-fitting global galaxy metallicity (Z) estimation is based on the SDSS photometric and spectroscopic data, and uses the FSPS code by Conroy et al. (2009).

Table 10. The number ratios of SN types in low- and high-luminosity bins of hosts, and the significance value P_B of the difference between the ratios in the two subsamples. The total number of SNe is 692 in 608 host galaxies.

	$M_g > -20.7$	$M_g \leq -20.7$	P_B
N_{Ia}/N_{CC}	$0.39^{+0.05}_{-0.04}$	$0.48^{+0.06}_{-0.05}$	0.12
N_{Ibc}/N_{II}	$0.34^{+0.05}_{-0.04}$	$0.39^{+0.06}_{-0.05}$	0.28
N_{Ic}/N_{Ib}	$1.76^{+0.58}_{-0.47}$	$2.53^{+0.82}_{-0.69}$	0.29

whole distribution is shifted (not scaled) towards the vertical axis to ease visual comparison. The large scatter of metallicity in the first three bins of morphology is attributed to the small numbers statistics of CC SNe host galaxies with the available SDSS data. As can be seen, even for our smaller subsample, the metallicity decreases not significantly from early- to late-type hosts, which reflects the observed mass–morphology (e.g. Nair & Abraham 2010a) and mass–metallicity (e.g. Tremonti et al. 2004) relations for spiral galaxies, predicting $\lesssim 0.5$ dex variations. Therefore, one may interpret the behaviour of N_{Ibc}/N_{II} ratio versus morphology as a possible reflection of the behaviour of global metallicity versus morphological type of spirals. However, we emphasize that any metallicity constraint from our analyses is very weak.

The dependence of the SNe number ratios on the global metallicity of the host galaxies previously was studied (e.g. Prantzos & Boissier 2003; Prieto, Stanek & Beacom 2008; Boissier & Prantzos 2009; Kelly & Kirshner 2012). Boissier & Prantzos (2009) derived global galaxy gas-phase metallicities (oxygen abundances), using the well-known metallicity–luminosity relation, and confirmed their earlier finding (Prantzos & Boissier 2003), namely that there is a positive correlation between N_{Ibc}/N_{II} and metallicity. The size of their sample did not allow firm conclusions about the N_{Ic}/N_{Ib} ratio. They explained these results using the following interpretation: with increasing galaxy metallicity (luminosity), the stellar envelope is lost more easily and lower mass stars may become SNe of Type Ibc (Ic), thus increasing the N_{Ibc}/N_{II} (N_{Ic}/N_{Ib}) ratio. Similar results were obtained for the N_{Ibc}/N_{II} versus metallicity relation by Prieto et al. (2008), who did not use the metallicity–luminosity relation but the directly measured metallicity for the hosts of 115 SNe from the SDSS DR4 in the redshift range of $0.01 < z < 0.04$. However, using spectra of 74 host H II regions, Anderson et al. (2010) found that the mean metallicity of immediate environments (which can be assumed to be more accurate) of SNe Ibc is not significantly higher (~ 0.06 dex) than that of SNe II. They suggested a possible metallicity sequence, in terms of increasing progenitor metallicity going from SNe II through SNe Ib and finally SNe Ic. Based on the sample of 20 well-observed SNe Ib/c, Leloudas et al. (2011) detected no significant difference between metallicities of immediate environments of Types Ic (higher in average by 0.08 dex) and Ib SNe. Modjaz et al. (2011) studied 35 SNe Ib/c obtaining significantly higher environmental metallicities for Type Ic SNe. However, Leloudas et al. (2011) noted that the results of Modjaz et al. (2011) were affected by the uncertainties in the individual metallicity measurements. Sanders et al. (2012) also found an insignificant difference between median metallicities from the spectra of immediate environments of 12 SNe Ib and 21 SNe Ic.

In addition, Boissier & Prantzos (2009) showed that the

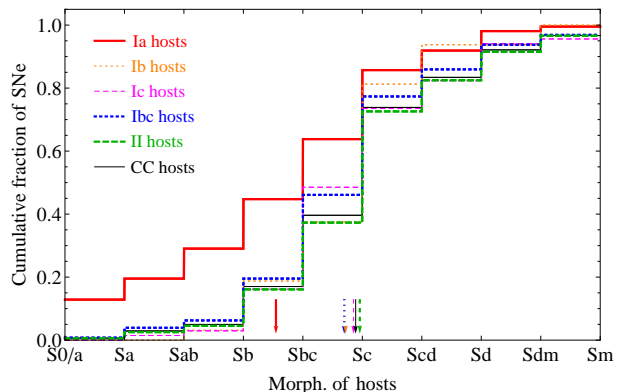


Figure 4. Cumulative fractions of the different types of SNe (692 events) versus host galaxy morphological type. The mean morphologies of host galaxies of each SNe type are shown by arrows.

Table 11. KS test probabilities of consistency for the distributions of hosts morphologies among different subsamples of SN types. The mean values of the morphological t -type and their errors are presented in parentheses.

Subsample 1		Subsample 2	P_{KS}
Ia (3.5 ± 0.1)	versus	Ib (4.7 ± 0.2)	0.04
Ia (3.5 ± 0.1)	versus	Ic (4.9 ± 0.2)	5×10^{-5}
Ia (3.5 ± 0.1)	versus	Ibc (4.7 ± 0.1)	8×10^{-6}
Ia (3.5 ± 0.1)	versus	II (5.0 ± 0.1)	8×10^{-10}
Ia (3.5 ± 0.1)	versus	CC (4.9 ± 0.1)	3×10^{-10}
Ib (4.7 ± 0.2)	versus	Ic (4.9 ± 0.2)	0.94
Ib (4.7 ± 0.2)	versus	II (5.0 ± 0.1)	0.85
Ic (4.9 ± 0.2)	versus	II (5.0 ± 0.1)	0.47
Ibc (4.7 ± 0.1)	versus	II (5.0 ± 0.1)	0.46

N_{Ia}/N_{CC} ratio increases with the metallicity of the host galaxies. However, they noted that the metallicities of SNe hosts simply reflect the observed mass–metallicity relation (e.g. Tremonti et al. 2004), and does not directly affect the N_{Ia}/N_{CC} ratio in contrast to the case of N_{Ibc}/N_{II} ratio. They suggest that it is the mass of hosts that affects the N_{Ia}/N_{CC} ratio.

In the above-mentioned studies, luminosities or metallicities of the galaxies were not defined for an individual morphological bin. Therefore, each luminosity or metallicity bin may have wide scatter of morphological types of the host galaxies. In this respect, to directly check the correlation of the number ratios of the different SN types with luminosity, one can also calculate the number ratios in two bins of low and high luminosities, independently of the morphology. Note that the luminosities are available for all the host galaxies, while the masses, for only about one-third of the sample. The SDSS g -band absolute magnitudes of galaxies were calculated using the data from Paper I. Table 10 shows the relative frequencies of SNe types in low- and high-luminosity bins. Sizes of the bins are constructed to include nearly equal numbers of all types of SNe in each bin. A similar analysis using the extracted metallicities of the host galaxies was not meaningful due to the smaller subsample (only 270 SNe have the host galaxies with a measured metallicity in the SDSS), as well as lower precision of the metallicity measurements compared to the luminosity measurements of the SNe hosts.

In Table 10, the $N_{\text{Ia}}/N_{\text{CC}}$ ratio appears to be higher for brighter, i.e., high-mass, galaxies. The result is in agreement with that of Boissier & Prantzos (2009). However, in both cases, the differences are not significant. The CC SNe are also equally distributed in these two bins. The $N_{\text{Ibc}}/N_{\text{II}}$ and $N_{\text{Ic}}/N_{\text{Ib}}$ ratios are not significantly higher in brighter galaxies. These results are similar to relative frequencies of CC SNe types versus M_{B} relations obtained by Boissier & Prantzos (2009) and Prantzos & Boissier (2003).

Despite the degree of subjectivity involved in the morphological classifications, the relations between the number ratios and morphology are probably tighter than those between the number ratios and luminosity or metallicity (see the significance values in Tables 8 and 10). Compared with the indirectly estimated metallicity, the morphological classification performed in Paper I using the combined g -, r -, and i -band images of the SDSS, i.e., considering to some extent also the colours of galaxies, is more closely related to the stellar population. It is also important to note that the ‘coloured’ morphological type of a galaxy is an observed parameter and is available for the nearby galaxies thanks to the SDSS imaging, while the sSFR and metallicity of a galaxy are inferred parameters based on synthetic models of the integrated broad-band fluxes or the spectra, and are affected by uncertainties due to dust contamination. Therefore, we choose to further consider mainly the observed quantities of the SNe host galaxies. In particular, we consider the morphology as the most important parameter shaping the number ratios of the different types of SNe.

Fig. 4 presents the cumulative distributions of the different SNe versus morphology of the host galaxies. In particular, 64 per cent of Type Ia SNe were discovered in S0/a–Sbc galaxies in contrast to 40 per cent of CC SNe. The mean morphological type of Ia SNe host galaxies is earlier than those of all types of CC SNe hosts (see t -types in Table 11 and the corresponding arrows in Fig. 4). A KS test shows that the distribution of morphologies for the hosts of Type Ia SNe is significantly different from those of hosts of all types of CC SNe (see Table 11). In contrast, the mean values and distributions of host morphologies for Type Ib, Ic, Ibc, and II SNe are nearly identical. Thus, Type Ia SNe, in contrast to CC SNe, are found more frequently in galaxies with older stellar populations.

3.2 Dependence of relative frequencies of SNe types on host barred structure

Given that bars in galactic stellar discs have an important influence on the star formation process of galaxies (e.g. Ellison et al. 2011), we study in this subsection the dependence of the relative frequencies of SNe types on the presence of bars in spiral host galaxies. Table 12 shows the distribution of the number ratios of SN types after separating the hosts into unbarred and barred types. There is no significant difference between the $N_{\text{Ia}}/N_{\text{CC}}$ ratios in the two subsamples. However, the $N_{\text{Ibc}}/N_{\text{II}}$ ratio is higher, with barely significance, in unbarred hosts compared with the ratio in barred hosts. The $N_{\text{Ic}}/N_{\text{Ib}}$ ratio is higher, but not significantly, in barred hosts compared with that in unbarred ones.

To explain the behaviours of the number ratios of the different SN types depending on the existence of bar, we analyse the morphological distributions of host galaxies with and without bars. Fig. 5 shows the distribution of the various types of SNe in hosts with or without bars for the different morphological types. The histograms illustrate that the distribution of SNe in barred galaxies is bimodal with respect to host-galaxy morphology, with peaks near Sbc and Sd types (see also Table 4). In contrast, the distribution of

Table 12. The number ratios of SN types in unbarred and barred hosts, and the significance value P_{B} of the difference between the ratios in the two subsamples.

	Unbarred	Barred	P_{B}
$N_{\text{Ia}}/N_{\text{CC}}$	$0.42^{+0.05}_{-0.04}$	$0.47^{+0.08}_{-0.06}$	0.31
$N_{\text{Ibc}}/N_{\text{II}}$	$0.40^{+0.05}_{-0.04}$	$0.28^{+0.07}_{-0.05}$	0.07
$N_{\text{Ic}}/N_{\text{Ib}}$	$1.92^{+0.51}_{-0.43}$	$2.86^{+1.31}_{-1.07}$	0.29

SNe in unbarred galaxies has a single peak towards Sc type. A KS test shows that the distributions of morphologies of host galaxies of all types of SNe with and without bars are significantly different ($P_{\text{KS}} = 6 \times 10^{-6}$) despite similar mean values for both distributions (see arrows in the top panel of Fig. 5). A similar distribution of SNe host galaxies was already seen in fig. 8 of Paper I.

Moreover, a bimodal distribution of barred galaxies was also found by Nair & Abraham (2010b), who recently released a morphological catalogue of 14034 visually classified galaxies ($0.01 < z < 0.1$) from the SDSS (Nair & Abraham 2010a). They noted that the bar fraction is bimodal with disc galaxy colour, having peaks towards the redder and bluer galaxies. The authors suggested that this trend may reveal two distinct types of bars: strong bars, that are more common in early-type, massive, redder, and gas-poor discs, and weak bars, that are frequently found in late-type, low-mass, bluer, and gas-rich spirals. Also based on the SDSS, but using instead the length of bars measured in nearby galaxies from the EFIGI⁹ catalogue (Baillard et al. 2011), a multiwavelength data base of visually classified 4458 PGC galaxies, de Lapparent et al. (2011) found that the fraction of barred galaxies is bimodal with a strong peak for type Sab, and a weaker one for type Sd (see their fig. 9).

To check the consistency of bar detection in our sample with that of the EFIGI catalogue, we make a subsample of galaxies (231 objects) that are common to both EFIGI and to our sample of SNe hosts. We compare the EFIGI `Bar Length` attribute with our detection (bar or no bar). When the `Bar Length` is 0, 2, 3, or 4, our bar detection is different for only 4 per cent of cases. However, we do not detect bars in 62 per cent of cases when `Bar Length` is 1. The EFIGI `Bar Length` = 1 mainly corresponds to the threshold of our bar detection. Moreover, to compare the bar fractions in the SNe hosts and the EFIGI catalogue within each morphological type, we limit the galaxies in both samples to the same distances and exclude the edge-on ($80^\circ \leq i \leq 90^\circ$) galaxies and those with completely distorted profiles (mergers and post-mergers/remnants) from both samples. The bar fractions per morphological type are in agreement with those of the EFIGI within our larger errors and taking into account that the detection of bar for `Bar Length` = 1 is somewhat different.

Thus, the unbarred and barred spirals have ‘specific’ distributions with morphology, consequently shaping the SNe distributions in these galaxies.

In particular, the $N_{\text{Ia}}/N_{\text{CC}}$ ratios in galaxies with and without bars are nearly equal, because the reduced ratio in barred galaxies from the second Sd–Sdm peak is somewhat compensated by the increased ratio in S0/a–Sc barred hosts (see the upper panel of Fig. 5 and Table 9). The situation is different for the $N_{\text{Ibc}}/N_{\text{II}}$ ratio be-

⁹ Extraction de Formes Idéalisées de Galaxies en Imagerie.

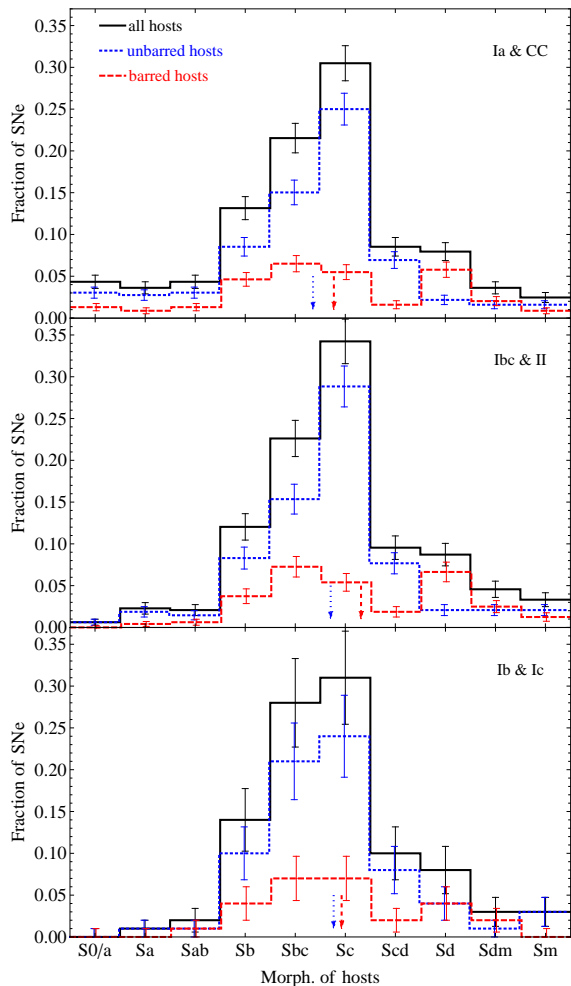


Figure 5. Fraction of SNe in galaxies with (red dashed lines) and without (blue dotted lines) bars, and their sum (black solid lines) versus host galaxy morphological type. The distributions of all (Ia and CC), CC (Ibc and II), and Ib plus Ic SNe are presented in the upper, middle, and bottom panels, respectively. The error bars assume a Poisson distribution (with ± 1 object if none is found). The mean morphologies of host galaxies with and without bars are shown by arrows.

cause the reduced ratio in the second peak of barred hosts is not compensated, due to a deficiency of CC SNe in S0/a–Sab hosts (see the middle panel of Fig. 5 and Table 9). The N_{Ic}/N_{Ib} ratio is somewhat higher, but not significantly, in subsample of barred galaxies than in unbarred ones, because of relatively weak contribution of SNe Ib from the barred spirals and particularly from the second peak (see the bottom panel of Fig. 5 and Table 3). In barred galaxies, we have five Ib SNe only in Sbc–Sc hosts in comparison with two Ib SNe only in Sdm hosts. The lack of Ib SNe is attributed to the small numbers statistics of these events.

To exclude the dependence of the number ratios on morphology, we analyse the ratios in the most populated morphological bins, i.e., Sbc+Sc. We find that there is no significant difference in the various number ratios between unbarred ($N_{Ia}/N_{CC} = 0.30^{+0.05}_{-0.04}$ and $N_{Ibc}/N_{II} = 0.37^{+0.06}_{-0.05}$) and barred ($N_{Ia}/N_{CC} = 0.36^{+0.11}_{-0.07}$ and $N_{Ibc}/N_{II} = 0.36^{+0.13}_{-0.08}$) Sbc–Sc hosts, and the values of the number ratios are the same as those in Table 9. Thus, in

the whole sequence of spiral galaxies, the variation of the number ratios of SNe with the presence of a bar is due to the bimodality of the morphology distribution in barred galaxies.

3.3 Dependence of relative frequencies of SNe types on host disturbance

Galaxy–galaxy interactions are expected to be responsible for triggering massive star formation, especially in strongly disturbed galaxies (e.g. Di Matteo et al. 2005; Lotz et al. 2008). In this subsection, we study the impact of galaxy host interactions on the number ratio of the various SNe types, by using the morphological disturbances of the hosts, defined in Section 2 as normal, perturbed, interacting, merging and post-merging/remnant, and illustrated in Fig. 2. These levels of disturbance are arranged in an approximate chronological order, according to the different stages of interaction, and have their own time-scales and levels of star formation (e.g. Lotz et al. 2008). Table 13 presents the values of the N_{Ia}/N_{CC} and N_{Ibc}/N_{II} ratios as a function of disturbance level, and Fig. 6 is the corresponding graph. We do not calculate the N_{Ic}/N_{Ib} ratio due to insufficient number of Ib and Ic SNe per bin of disturbance.

From Table 13 and Fig. 6, the N_{Ia}/N_{CC} ratio is at a nearly constant level when moving from the normal, perturbed to the interacting galaxies. Then it slightly declines in the merging galaxies and jumps to the highest value in the post-merging/remnant host galaxies. Only the difference between the N_{Ia}/N_{CC} ratios in the merging and post-merging/remnant hosts is statistically significant ($P_B = 2 \times 10^{-3}$). Within 10 hosts in the merging subsample, there are only three Ia and 14 CC SNe, and in 17 post-merging/remnant galaxies, 12 Ia and six CC SNe.

The most likely reason for relative overpopulation of CC SNe in merging spiral galaxies is that these galaxies are dominated by violent starbursts (e.g. Lambas et al. 2012), particularly in their circumnuclear regions (e.g. Storch-Bergmann et al. 2001). During the relatively short time-scale of the merging stage (~ 0.5 Gyr), as predicted by numerical simulations (e.g. Di Matteo et al. 2005; Lotz et al. 2008), the spiral, gas-rich galaxies do not have enough time to produce many Type Ia SNe (lifetime > 0.5 Gyr), but can intensively produce CC SNe, assuming short lifetimes for the CC SNe progenitors (lifetime < 0.1 Gyr). Moreover, the positions of CC SNe in our merging hosts mostly coincide with circumnuclear regions and only in few cases with bright H II regions, which is in agreement with the previously found central excess of CC SNe in extremely disturbed or merging galaxies (e.g. Haberman et al. 2010, 2012; Anderson et al. 2011; Herrero-Illana et al. 2012).

In our sample, the observed number of post-merging/remnant hosts is higher than the observed number of merging hosts most probably due to the longer time-scale of the latter stage of interaction ($\gtrsim 1$ Gyr; e.g. Di Matteo et al. 2005; Lotz et al. 2008). The post-merging/remnant galaxies have enough time to produce many Type Ia SNe, but not enough high-mass star formation to produce sufficient number of CC SNe. In the simulations of galaxy–galaxy interactions, the majority of post-merging galaxies, and especially the merger remnants, are observed after the final coalescence with a significant loss of gas content (e.g. Di Matteo et al. 2005; Lotz et al. 2008). Their SFRs are consistent with the SFRs of early-type spirals (e.g. Lotz et al. 2008), in which we observe more Type Ia than CC SNe (see Table 3). It is important to note that some of the merger remnant galaxies in very late stages of interaction can be classified as normal early-type galaxies because of visual similarities (see also figs. 1 and 2 of Lotz et al. 2008). For instance, in our sample of normal galaxies, there are seven hosts of

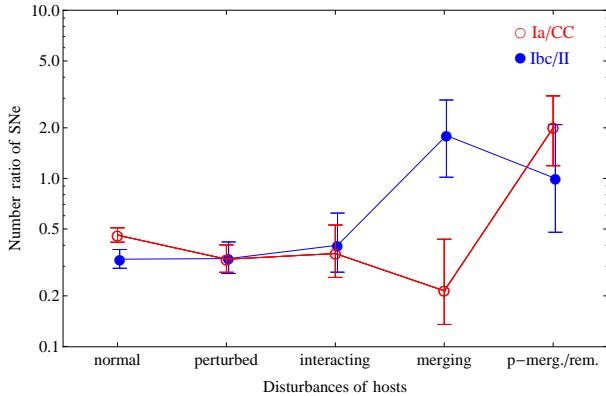


Figure 6. Relative frequency of SNe types as a function of the disturbance level of host galaxies.

Table 13. The number ratios of SN types according to the disturbance level of host galaxies. The total number of SNe is 692 in 608 host galaxies.

	normal	perturbed	interacting	merging	p-merg./rem.
N_{Ia}/N_{CC}	$0.46^{+0.05}_{-0.04}$	$0.33^{+0.07}_{-0.05}$	$0.36^{+0.17}_{-0.10}$	$0.21^{+0.22}_{-0.08}$	$2.00^{+1.10}_{-0.81}$
N_{Ibc}/N_{II}	$0.33^{+0.05}_{-0.04}$	$0.33^{+0.09}_{-0.06}$	$0.40^{+0.22}_{-0.12}$	$1.80^{+1.13}_{-0.78}$	$1.00^{+1.09}_{-0.52}$

S0/a–Sab types that are also flagged as possible merger remnants in late stages. Remarkably, there are eight SNe in these galaxies, all of Type Ia. Therefore, the true N_{Ia}/N_{CC} ratio could be even higher than measured here for the post-merging/remnant subsample.

The N_{Ibc}/N_{II} ratio is nearly constant when moving from the normal, and perturbed to the interacting hosts. Then, in contrast to the N_{Ia}/N_{CC} ratio, it jumps to its highest value in the merging galaxies and subsequently slightly declines in the post-merging/remnant subsample. Within seven hosts of CC SNe in the merging subsample, there are nine SNe Ibc and five SNe II, and in six post-merging/remnant hosts of CC SNe, only three SNe Ibc and three SNe II. Only the difference of the N_{Ibc}/N_{II} ratios between the interacting and merging hosts is statistically significant ($P_B = 0.02$).

Despite the small numbers statistics, we speculate that the remarkable excess of SNe Ibc within the central regions of strongly disturbed or merging galaxies (e.g. Habergham et al. 2010, 2012; Anderson et al. 2011; Nazaryan et al. 2013) is responsible for the observed high value of the N_{Ibc}/N_{II} ratio in the merging subsample. We find that the merging galaxies hosting CC SNe are more luminous than the normal ones (a KS test probability is only 0.03 that they are drawn from the same distribution) by almost 0.4 mag in the mean of M_g . One may interpret this as a possible implication for somewhat higher metallicity in these galaxies (~ 0.05 dex from Tremonti et al. 2004). However, in the central regions of merging galaxies where the excess of Ibc SNe is observed, metallicities are systematically lower (~ 0.2 dex from Kewley et al. 2006) than those of normal and weakly interacting galaxies. The possible roles of metallicity, age, fraction of binary systems, and IMF shape are discussed in detail in Anderson et al. (2011, 2012), Habergham et al. (2012), and Kangas et al. (2013). In the final stage of interactions, i.e. in the post-merging/remnant galaxies, the observed trend of the N_{Ibc}/N_{II} ratio probably is

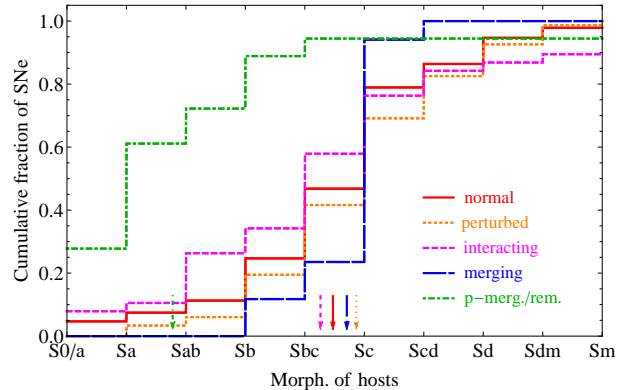


Figure 7. Cumulative fraction of 692 SNe versus host galaxy morphological type. The mean morphologies of host galaxies of each type of disturbance are shown by arrows.

Table 14. KS test probabilities of consistency for the distributions of hosts morphologies among the different subsamples by disturbance level. The t -type mean values and errors of the means are presented in parentheses.

	Subsample 1	Subsample 2	P_{KS}
Normal	(4.5 ± 0.1)	versus Perturbed	(4.9 ± 0.1) 0.23
Perturbed	(4.9 ± 0.1)	versus Interacting	(4.3 ± 0.4) 0.17
Interacting	(4.3 ± 0.4)	versus Merging	(4.7 ± 0.2) 0.12
Merging	(4.7 ± 0.2)	versus p-merg./rem.	(1.8 ± 0.5) 6×10^{-6}
p-merg./rem.	(1.8 ± 0.5)	versus Normal	(4.5 ± 0.1) 10^{-6}

caused by the continuous decrease of both gas fraction and high-mass star formation (e.g. Di Matteo et al. 2005; Lotz et al. 2008).

We investigate also how the interaction of galaxies affects the morphological type of host galaxies. Fig. 7 presents the cumulative distributions of morphologies of the hosts of 692 SNe for the different disturbance levels. The mean morphological type of post-merging/remnant hosts is considerably earlier than those of all mean types of hosts in different stages of interaction (see t -types in Table 14 and arrows in Fig. 7). A KS test shows that the distribution of morphology of post-merging/remnant hosts is significantly different from those of the preceding (merging) and following (normal) stages (see Table 14). The mean values and distributions of morphological types of normal, perturbed, interacting, and merging hosts are not significantly different from one another. Thus, the mean morphological classification of the host galaxies is strongly affected in the final stage of galaxy–galaxy interaction, respectively, affecting also the number ratios of SNe types.

A similar behaviour of morphology is predicted in the simulations of interactions: the initial galaxies with late-type disc morphologies become perturbed during the first passage, reach both the maximum morphological disturbances and SFR at the final merger, then the post-merger and remnant galaxies gradually end up with early-type disc morphologies and gas content (e.g. Di Matteo et al. 2005; Lotz et al. 2008). We understand that although the duration and strength of the observed morphological disturbances and SFRs depend on the mass, merger orientation, and orbital parameters, the gas properties of the initial galaxies, and the presence of dust (see the detailed discussion in Lotz et al. 2008), the presented simpli-

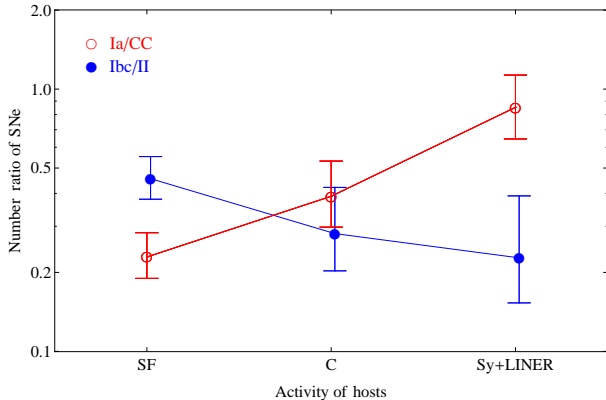


Figure 8. Relative frequency of SNe types as a function of activity classes of their host galaxies. The BPT activity classes are available only for 232 hosts with 268 SNe.

Table 15. The number ratios of SN types for host galaxies with different activity classes. The BPT activity classes are available only for 232 hosts with 268 SNe.

	SF	C	Sy+LINER	All
N_{Ia}/N_{CC}	$0.23^{+0.05}_{-0.04}$	$0.39^{+0.14}_{-0.09}$	$0.85^{+0.28}_{-0.21}$	$0.35^{+0.05}_{-0.04}$
N_{Ibc}/N_{II}	$0.46^{+0.10}_{-0.08}$	$0.28^{+0.14}_{-0.08}$	$0.23^{+0.16}_{-0.07}$	$0.38^{+0.07}_{-0.05}$

fied model qualitatively explains the obtained results of the relative frequencies of SNe types.

3.4 Dependence of relative frequencies of SNe types on host activity class

Given that nuclear activity of galaxies is often correlated with the star formation in discs of spiral galaxies (e.g. Kauffmann et al. 2003, 2007; Knapen 2005; Popović et al. 2009), we examine in this subsection the influence of the nuclear activity of the hosts on the number ratios of the different SN types.

In Table 15, for 268 SNe in 232 host galaxies with available BPT activity data, we calculate the number ratios by binning the SNe hosts according to their activity class. The Sy and LINER bins are merged due to an insufficient number of Type Ibc SNe in the Sy bin. As in the previous subsections, the number of events is insufficient to evaluate the N_{Ic}/N_{Ib} ratio in the subsamples with available activity classes. Fig. 8 presents the relative frequency of SNe types as a function of activity classes of their host galaxies.

Fig. 8 shows that the N_{Ia}/N_{CC} ratio increases when moving from SF, C, to Sy+LINER classes. The differences between the N_{Ia}/N_{CC} ratios in SF versus C ($P_B = 0.04$) and C versus Sy+LINER ($P_B = 0.03$) subsamples are statistically significant. In addition, the mean of $1/sSFR$ for the SNe hosts obtained from the SDSS is significantly higher for Sy+LINER galaxies and lower for SF galaxies.

The N_{Ibc}/N_{II} ratio decreases not significantly when moving from SF, C, to Sy+LINER classes. The host galaxies with Sy+LINER activity classes are more luminous than the hosts in C bin, which are in turn more luminous than the hosts in SF subsample: the difference in the mean of M_g between Sy+LINER and C subsamples is about 0.2 mag, while it is about 0.5 mag between

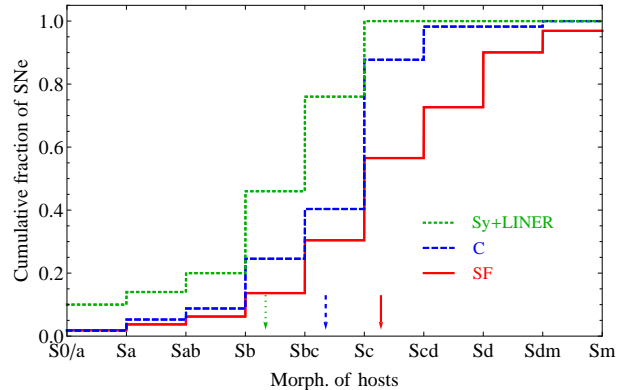


Figure 9. Cumulative fraction of 268 SNe versus host galaxy morphological type. The mean morphologies of host galaxies of each activity class of nucleus are shown by arrows.

Table 16. KS test probabilities of consistency for the distributions of hosts morphologies among the different subsamples of activity classes. The t -type mean values and errors of the means are presented in parentheses.

	Subsample 1	Subsample 2	P_{KS}
SF	(5.3 ± 0.1) versus C	(4.4 ± 0.2)	6×10^{-4}
C	(4.4 ± 0.2) versus Sy+LINER	(3.3 ± 0.2)	2×10^{-3}
Sy+LINER	(3.3 ± 0.2) versus SF	(5.3 ± 0.1)	3×10^{-7}

the C and SF subsamples. A KS test yields probabilities of 0.05 and 4×10^{-3} , respectively, that the luminosities are drawn from the same distribution. The trend for luminosity of the hosts can be true also for their metallicities, however the metallicities extracted from the SDSS do not allow us to check the mentioned behaviour directly. Again, we emphasize that any metallicity constraint from our analyses is unconvincing.

As in previous subsections, Fig. 9 presents the cumulative distributions of morphologies of the hosts of 268 SNe according to their activity classes. The mean morphological type of Sy+LINER hosts is earlier by nearly one type than that of C class of hosts, whose mean morphology is in turn earlier than that of SF hosts by also nearly one type (see t -types in Table 16 and arrows in Fig. 9). In our sample, only 20 ± 10 per cent of Sy+LINER hosts have a level of disturbance different from normal, whereas about 40 ± 8 per cent of hosts in each C and SF bins have disturbed morphology.

The behaviour of the number ratios of SNe types can be explained by the existence of a time delay between the interaction and the setting of the different classes of activity: an interaction induces first the SF, then C, and finally the AGN (Sy+LINER) stages of galaxies (e.g. Sabater et al. 2013). In this scenario, the interaction is responsible for the morphological disturbance and inflow of gas towards the centre, which first triggers star formation (e.g. Storch-Bergmann et al. 2001; Sabater et al. 2013) and increases the $sSFR$ (e.g. Lotz et al. 2008). Therefore, in the SF stage, we observe a lower value of the N_{Ia}/N_{CC} ratio and at the same time a somewhat higher value of the N_{Ibc}/N_{II} ratio as in the morphologically disturbed (interacting/merging) subsample of late-type galaxies (see Tables 8, 9, and 13). The starburst then fades with time and the C (composite of SF and AGN) class evolves to the AGN (Sy+LINER) class (time-scale $\sim 0.3 - 0.5$ Gyr; Wild et al. 2010)

with a comparatively relaxed disturbance, early-type morphology, poor gas fraction, and old stellar population. Therefore, in the AGN stage, we observe inverse values of the ratios as in morphologically less disturbed (relaxed) early-type galaxies (see Tables 8, 9, and 13).

Again, we suggest, that even if not considering the above-mentioned scenario, the morphologies, in combination with the disturbance levels, can be considered as the most important parameter shaping the number ratios of the different types of SNe in host galaxies with various classes of activity.

3.5 Selection effects and possible sample biases

There are various selection effects and observational biases that might potentially affect our study: SN spectroscopic type, host-galaxy morphology and magnitude biases depending on distance, inclination effects of the host galaxy disc, Shaw effect depending on the radial distance of SNe in galaxies, inclusion of uncertain, peculiar or transient types of SNe into the study, methods of SNe discovery (photographic or CCD imaging), the SDSS spectroscopic fibre bias, etc. For more details, the reader is referred to Paper I, where many of these effects are discussed.

To check the impact of the mentioned effects on the results of our study, we repeated the analyses presented in previous subsections using different subsamples of SNe and their host galaxies, by dividing them according to the galaxy distance, or selecting only SNe discovered since the use of CCDs (after 2000), or analysing only SNe which exploded far from the circumnuclear regions of host galaxies, or considering only SNe without uncertain, peculiar or transient types. There are only one superluminous SN (from the sample of Quimby et al. 2013), four peculiar calcium-rich transients (from the sample of Yuan et al. 2013), and six peculiar Type Iax SNe (from the sample of Foley et al. 2013). We note that our subsample of Type II SNe includes 33 Type IIb and 43 Type IIn SNe. They have the same distribution according to the host morphology as Type II SNe (see also table 5 of Paper I). Despite the smaller sizes and larger error bars of the number ratios of SNe types in the constructed subsamples, the various trends of the number ratios remain the same qualitatively.

Note that we may have missed weak bars because of inclination effects, or that in some cases the SDSS images of the hosts may be too shallow and insufficiently resolved to detect bars (see also Paper I). For instance, among the spiral host galaxies with inclinations $i \leq 50^\circ$, the average bar fraction is 40 ± 5 per cent, whereas for hosts without inclination limit, the average bar fraction is 30 ± 3 per cent. By selecting only galaxies with inclinations $i \leq 50^\circ$, we verify that this effect does not bias the trends of the number ratios presented in Section 3.2.

Similarly, the restriction of the SNe hosts with activity classes to inclinations $i \leq 50^\circ$ gives us the possibility to avoid contamination in determination of the activity classes of nuclei, namely when the circumnuclear regions of galaxies are veiled by part of a dense and opaque disc. This effect is weak in our sample and does not qualitatively affect the trends presented in Section 3.4.

It is also important to note that the observed numbers and volumetric rates of SNe may be somewhat different from those predicted from the cosmic SFR (see discussions in Horiuchi & Beacom 2010 and Horiuchi et al. 2011). However, the mentioned difference may affect just the overall scales of the number ratios, but not affect any comparisons between the number ratios in different galaxy subsamples.

Summarizing, we conclude that there are no strong selection

effects and biases within our SNe and host galaxies samples, which could drive the observed behaviours of the relative frequencies of SNe types in the spiral host galaxies presented in this study.

4 CONCLUSIONS

In this second paper of a series, using a well-defined and homogeneous sample of host galaxies from the SDSS, presented in the first paper (Hakobyan et al. 2012), we analyse the number ratios of different SN types ($N_{\text{Ia}}/N_{\text{CC}}$, $N_{\text{Ibc}}/N_{\text{II}}$, and $N_{\text{Ic}}/N_{\text{Ib}}$) in spirals with various morphologies and in barred or unbarred galaxies. We also explore the variations in the number ratios with different levels of morphological disturbance of the hosts. Our sample consists of 608 spiral galaxies, which host 692 SNe in total. In addition, we perform a statistical study of 268 SNe discovered in 232 galaxies with available activity classes of nucleus (SF, C, and Sy+LINER). We propose that the underlying mechanisms shaping the number ratios of SNe types can be interpreted within the framework of interaction-induced star formation, in addition to the known relations between morphologies and stellar populations.

The results obtained in this article are summarized below, along with their interpretations.

(i) We find a strong trend in the behaviour of $N_{\text{Ia}}/N_{\text{CC}}$ depending on host-galaxy morphological type, such that early-type (high-mass or high-luminosity) spirals include proportionally more Type Ia SNe. In addition, there is a strong trend in the distribution of $1/\text{sSFR}$, such that sSFR of host galaxies systematically increases from early- to late-type spirals. The behaviour of $N_{\text{Ia}}/N_{\text{CC}}$ versus morphology is a simple reflection of the behaviour of $1/\text{sSFR}$ versus morphological types of galaxies.

(ii) The $N_{\text{Ibc}}/N_{\text{II}}$ ratio is higher in a broad bin of early-type hosts. The $N_{\text{Ibc}}/N_{\text{II}}$ distribution is consistent within errors with the metallicity distribution of the host galaxies, and shows a mild variation with morphology of the hosts. In addition, the $N_{\text{Ibc}}/N_{\text{II}}$ and $N_{\text{Ic}}/N_{\text{Ib}}$ ratios are higher, not significantly, in more luminous (metal-rich) host galaxies. However, any metallicity constraint from our analyses is very weak.

(iii) The mean morphological type of spiral galaxies hosting Type Ia SNe is significantly earlier than the mean host type for all other types of CC SNe, which are, in contrast, consistent with one another.

(iv) There is no difference between the $N_{\text{Ia}}/N_{\text{CC}}$ ratios in the subsamples of unbarred and barred spirals. However, the $N_{\text{Ibc}}/N_{\text{II}}$ ratio is higher, with barely significance, in unbarred hosts in comparison with the same ratio in barred hosts. The number ratios of SNe in barred galaxies are caused by the bimodal distribution (two distinct types of bars) of these galaxies with morphology. We find that in an individual morphological bin, there is no any significant difference in the various number ratios between the unbarred and barred hosts.

(v) The $N_{\text{Ia}}/N_{\text{CC}}$ ratio is nearly constant when changing from normal, perturbed to interacting galaxies, then declines in merging galaxies, whereas it jumps to the highest value in post-merging/remnant host galaxies. During the relatively short time-scale of the merging stage, the spiral, gas-rich galaxies do not have enough time to produce many Type Ia SNe, but can intensively produce CC SNe, assuming short lifetimes for the CC SNe progenitors. In the post-merging/remnant galaxies with longer time-scale, the SFRs and morphologies of host galaxies are strongly affected, significantly increasing the $N_{\text{Ia}}/N_{\text{CC}}$ ratio.

(vi) The $N_{\text{Ibc}}/N_{\text{II}}$ ratio is nearly constant when changing from normal, perturbed to interacting galaxies, then jumps to the highest value in merging galaxies and slightly declines in post-merging/remnant subsample. In our merging hosts, the positions of CC SNe, particularly SNe of Ibc type, mostly coincide with the circumnuclear regions and only in few cases with bright H II regions, which is in agreement with the previously found central excess of CC SNe in extremely disturbed or merging galaxies.

(vii) The $N_{\text{Ia}}/N_{\text{CC}}$ ($N_{\text{Ibc}}/N_{\text{II}}$) ratio increases (decreases) when moving from SF, C, to Sy+LINER activity classes (BPT) for the host galaxies. In the invoked scenario, the interaction is responsible for morphological disturbances and for partially sending gas inward, which first triggers star formation and increases sSFR. Therefore, in the SF stage, we observe a lower value of the $N_{\text{Ia}}/N_{\text{CC}}$ ratio and a somewhat higher value of the $N_{\text{Ibc}}/N_{\text{II}}$ ratio as in morphologically disturbed (interacting or merging) late-type galaxies. The starburst then fades with time and the C (composite of SF and AGN) class evolves to the AGN (Sy+LINER) with a comparatively relaxed disturbance, early-type morphology, poor gas fraction, and old stellar population. Therefore, in the AGN stage, we observe inverse values of the ratios as in morphologically less disturbed (relaxed) early-type galaxies.

We are not able to discriminate between the natures of different CC SNe progenitors because the time-scales of both the interaction stages and activity classes of nucleus are much longer than the upper limits of progenitor lifetimes of Types Ibc and II SNe discussed in the Introduction. In the forthcoming third paper of this series (Aramyan et al. in preparation), we study the distributions of the different types of SNe relative to the spiral arms of the host galaxies with various morphologies, in order to understand the relationship between the nature of SNe progenitors and arm-induced star formation.

ACKNOWLEDGEMENTS

AAH, ARP, and LSA acknowledge the hospitality of the Institut d’Astrophysique de Paris (France) during their stay as visiting scientists supported by the Collaborative Bilateral Research Project of the State Committee of Science (SCS) of the Republic of Armenia and the French Centre National de la Recherche Scientifique (CNRS). This work was supported by State Committee Science MES RA, in frame of the research project number SCS 13–1C013. AAH is also partially supported by the ICTP. VZA and JMG are supported by grants SFRH/BPD/70574/2010 and SFRH/BPD/66958/2009 from FCT (Portugal), respectively. VZA would further like to thank for the support by the ERC under the FP7/EC through a Starting Grant agreement number 239953. DK acknowledges financial support from the Centre National d’Études Spatiales (CNES). MT is partially supported by the PRIN-INAF 2011 with the project Transient Universe: from ESO Large to PESSTO. This work was made possible in part by a research grant from the Armenian National Science and Education Fund (ANSEF) based in New York, USA. Finally, we are especially grateful to our referee for his/her constructive comments. Funding for SDSS–III has been provided by the Alfred P. Sloan Foundation, the Participating Institutions, the National Science Foundation, and the US Department of Energy Office of Science. The SDSS–III web site is <http://www.sdss3.org/>. SDSS–III is managed by the Astrophysical Research Consortium for the Participating Institutions of the SDSS–III Collaboration including the University of Arizona, the Brazilian Participation Group, Brookhaven National Laboratory,

University of Cambridge, University of Florida, the French Participation Group, the German Participation Group, the Instituto de Astrofísica de Canarias, the Michigan State/Notre Dame/JINA Participation Group, Johns Hopkins University, Lawrence Berkeley National Laboratory, Max Planck Institute for Astrophysics, New Mexico State University, New York University, Ohio State University, Pennsylvania State University, University of Portsmouth, Princeton University, the Spanish Participation Group, University of Tokyo, University of Utah, Vanderbilt University, University of Virginia, University of Washington, and Yale University.

REFERENCES

- Ahn C. P. et al., 2014, *ApJS*, 211, 17
 Alberdi A., Colina L., Torrelles J. M., Panagia N., Wilson A. S., Garrington S. T., 2006, *ApJ*, 638, 938
 Anderson J. P., Covarrubias R. A., James P. A., Hamuy M., Habergham S. M., 2010, *MNRAS*, 407, 2660
 Anderson J. P., Habergham S. M., James P. A., 2011, *MNRAS*, 416, 567
 Anderson J. P., Habergham S. M., James P. A., Hamuy M., 2012, *MNRAS*, 424, 1372
 Anderson J. P., James P. A., 2009, *MNRAS*, 399, 559
 Aramyan L. S., Petrosian A. R., Hakobyan A. A., Mamon G. A., Kunth D., Turatto M., Adibekyan V. Z., Nazaryan T. A., 2013, *Astrophysics*, 56, 153
 Baillard A. et al., 2011, *A&A*, 532, A74
 Baldwin J. A., Phillips M. M., Terlevich R., 1981, *PASP*, 93, 5
 Barnard G. A., 1945, *Nature*, 156, 177
 Bartunov O. S., Makarova I. N., Tsvetkov D. Y., 1992, *A&A*, 264, 428
 Blanc N. et al., 2005, *The Astronomer’s Telegram*, 532, 1
 Boissier S., Boselli A., Prantzos N., Gavazzi G., 2001, *MNRAS*, 321, 733
 Boissier S., Prantzos N., 2009, *A&A*, 503, 137
 Bressan A., Della Valle M., Marziani P., 2002, *MNRAS*, 331, L25
 Cameron E., 2011, *PASA*, 28, 128
 Cappellaro E., Evans R., Turatto M., 1999, *A&A*, 351, 459
 Conley A. et al., 2008, *ApJ*, 681, 482
 Conroy C., Gunn J. E., White M., 2009, *ApJ*, 699, 486
 Crowther P. A., 2013, *MNRAS*, 428, 1927
 Das M., Sengupta C., Ramya S., Misra K., 2012, *MNRAS*, 423, 3274
 Davies R. I., Müller Sánchez F., Genzel R., Tacconi L. J., Hicks E. K. S., Friedrich S., Sternberg A., 2007, *ApJ*, 671, 1388
 de Lapparent V., Baillard A., Bertin E., 2011, *A&A*, 532, A75
 Di Matteo T., Springel V., Hernquist L., 2005, *Nature*, 433, 604
 Eldridge J. J., Izzard R. G., Tout C. A., 2008, *MNRAS*, 384, 1109
 Eldridge J. J., Langer N., Tout C. A., 2011, *MNRAS*, 414, 3501
 Ellison S. L., Mendel J. T., Patton D. R., Scudder J. M., 2013, *MNRAS*, 435, 3627
 Ellison S. L., Nair P., Patton D. R., Scudder J. M., Mendel J. T., Simard L., 2011, *MNRAS*, 416, 2182
 Filippenko A. V., 1997, *ARA&A*, 35, 309
 Filippenko A. V., Matheson T., 1993, *IAU Circ.*, 5842, 2
 Foley R. J. et al., 2013, *ApJ*, 767, 57
 Foley R. J., Mandel K., 2013, *ApJ*, 778, 167
 Förster F., Schawinski K., 2008, *MNRAS*, 388, L74
 Habergham S. M., Anderson J. P., James P. A., 2010, *ApJ*, 717, 342

- Habergham S. M., James P. A., Anderson J. P., 2012, *MNRAS*, 424, 2841
- Hakobyan A. A., 2008, *Astrophysics*, 51, 69
- Hakobyan A. A., Adibekyan V. Z., Aramyan L. S., Petrosian A. R., Gomes J. M., Mamon G. A., Kunth D., Turatto M., 2012, *A&A*, 544, A81
- Hakobyan A. A., Mamon G. A., Petrosian A. R., Kunth D., Turatto M., 2009, *A&A*, 508, 1259
- Hakobyan A. A. et al., 2011, *Astrophysics*, 54, 301
- Hakobyan A. A., Petrosian A. R., McLean B., Kunth D., Allen R. J., Turatto M., Barbon R., 2008, *A&A*, 488, 523
- Hamuy M., 2003, arXiv: astro-ph/0301006
- Heger A., Fryer C. L., Woosley S. E., Langer N., Hartmann D. H., 2003, *ApJ*, 591, 288
- Herrero-Illana R., Pérez-Torres M. Á., Alberdi A., 2012, *A&A*, 540, L5
- Hopkins P. F., 2012, *MNRAS*, 420, L8
- Hopkins P. F., Quataert E., 2010, *MNRAS*, 407, 1529
- Horiuchi S., Beacom J. F., 2010, *ApJ*, 723, 329
- Horiuchi S., Beacom J. F., Kochanek C. S., Prieto J. L., Stanek K. Z., Thompson T. A., 2011, *ApJ*, 738, 154
- James P. A., Anderson J. P., 2006, *A&A*, 453, 57
- Jarrett T. H. et al., 2006, *AJ*, 131, 261
- Kangas T., Mattila S., Kankare E., Kotilainen J. K., Väisänen P., Greimel R., Takalo A., 2013, *MNRAS*, 436, 3464
- Kankare E., 2013, PhD thesis, University of Turku
- Kauffmann G. et al., 2007, *ApJS*, 173, 357
- Kauffmann G. et al., 2003, *MNRAS*, 346, 1055
- Kelly P. L., Kirshner R. P., 2012, *ApJ*, 759, 107
- Kewley L. J., Geller M. J., Barton E. J., 2006, *AJ*, 131, 2004
- Knapen J. H., 2005, *A&A*, 429, 141
- Kuo C.-Y., Lim J., Tang Y.-W., Ho P. T. P., 2008, *ApJ*, 679, 1047
- Lambas D. G., Alonso S., Mesa V., O'Mill A. L., 2012, *A&A*, 539, A45
- Leaman J., Li W., Chornock R., Filippenko A. V., 2011, *MNRAS*, 412, 1419
- Leloudas G. et al., 2011, *A&A*, 530, A95
- Li W., Chornock R., Leaman J., Filippenko A. V., Poznanski D., Wang X., Ganeshalingam M., Mannucci F., 2011, *MNRAS*, 412, 1473
- Lotz J. M., Jonsson P., Cox T. J., Primack J. R., 2008, *MNRAS*, 391, 1137
- Mannucci F., Della Valle M., Panagia N., Cappellaro E., Cresci G., Maiolino R., Petrosian A., Turatto M., 2005, *A&A*, 433, 807
- Maoz D., Mannucci F., 2012, *PASA*, 29, 447
- Milne P. A., Brown P. J., Roming P. W. A., Bufano F., Gehrels N., 2013, *ApJ*, 779, 23
- Modjaz M., Kewley L., Bloom J. S., Filippenko A. V., Perley D., Silverman J. M., 2011, *ApJ*, 731, L4
- Muñoz Marín V. M., González Delgado R. M., Schmitt H. R., Cid Fernandes R., Pérez E., Storchi-Bergmann T., Heckman T., Leitherer C., 2007, *AJ*, 134, 648
- Murdin P., Green D. W. E., 1988, *IAU Circ.*, 4546, 1
- Nair P. B., Abraham R. G., 2010a, *ApJS*, 186, 427
- Nair P. B., Abraham R. G., 2010b, *ApJ*, 714, L260
- Navasardyan H., Petrosian A. R., Turatto M., Cappellaro E., Boulesteix J., 2001, *MNRAS*, 328, 1181
- Nayak I. et al., 2011, *Central Bureau Electronic Telegrams*, 2694, 1
- Nazaryan T. A., Petrosian A. R., Hakobyan A. A., Adibekyan V. Z., Kunth D., Mamon G. A., Turatto M., Aramyan L. S., 2013, *Ap&SS*, 347, 365
- Petrosian A. et al., 2005, *AJ*, 129, 1369
- Petrosian A. R., Turatto M., 1990, *A&A*, 239, 63
- Petrosian A. R., Turatto M., 1995, *A&A*, 297, 49
- Podsiadlowski P., Joss P. C., Hsu J. J. L., 1992, *ApJ*, 391, 246
- Popović L. Č., Smirnova A. A., Kovačević J., Moiseev A. V., Afanasiev V. L., 2009, *AJ*, 137, 3548
- Prantzos N., Boissier S., 2003, *A&A*, 406, 259
- Prieto J. L., Stanek K. Z., Beacom J. F., 2008, *ApJ*, 673, 999
- Quimby R. M., Yuan F., Akerlof C., Wheeler J. C., 2013, *MNRAS*, 431, 912
- Richmond M. W., Filippenko A. V., Galisky J., 1998, *PASP*, 110, 553
- Sabater J., Best P. N., Argudo-Fernández M., 2013, *MNRAS*, 430, 638
- Sanders N. E. et al., 2012, *ApJ*, 758, 132
- Scannapieco E., Bildsten L., 2005, *ApJ*, 629, L85
- Schaller G., Schaerer D., Meynet G., Maeder A., 1992, *A&AS*, 96, 269
- Shao X. et al., 2014, *ApJ*, 791, 57
- Silk J., Norman C., 2009, *ApJ*, 700, 262
- Silverman J. M. et al., 2012, *MNRAS*, 425, 1789
- Smartt S. J., 2009, *ARA&A*, 47, 63
- Smartt S. J., Eldridge J. J., Crockett R. M., Maund J. R., 2009, *MNRAS*, 395, 1409
- Smith N., Li W., Filippenko A. V., Chornock R., 2011, *MNRAS*, 412, 1522
- Spergel D. N. et al., 2007, *ApJS*, 170, 377
- Storchi-Bergmann T., González Delgado R. M., Schmitt H. R., Cid Fernandes R., Heckman T., 2001, *ApJ*, 559, 147
- Tremonti C. A. et al., 2004, *ApJ*, 613, 898
- Turatto M., 2003, in Weiler K., ed., *Lecture Notes in Physics*, Berlin Springer Verlag Vol. 598, *Supernovae and Gamma-Ray Bursters*. pp 21–36
- van den Bergh S., 1997, *AJ*, 113, 197
- van den Bergh S., Li W., Filippenko A. V., 2005, *PASP*, 117, 773
- Wang J., Deng J. S., Wei J. Y., 2010, *MNRAS*, 405, 2529
- Wild V., Heckman T., Charlot S., 2010, *MNRAS*, 405, 933
- Wyse R. F. G., 2004, *ApJ*, 612, L17
- Yuan F., Kobayashi C., Schmidt B. P., Podsiadlowski P., Sim S. A., Scalzo R. A., 2013, *MNRAS*, 432, 1680

SUPPORTING INFORMATION

Additional Supporting Information may be found in the online version of this article:

(<http://mnras.oxfordjournals.org/lookup/suppl/doi:10.1093/mnras/stu1598/-/DC1>).